UNLIMITED

Trans 2197

DEFENCE RESEARCH AGENCY

Library Translation 2197

March 1992

An Experimental Study of Transition and Leading Edge Contamination on Swept Wings

by

D. Arnal
J.C. Juillen

Farnborough, Hampshire

DEFENCE RESEARCH AGENCY
Aerospace Division
RAE Farnborough

Library Translation 2197

Received for printing 12 March 1992

THE EXPERIMENTAL STUDY OF TRANSITION AND LEADING EDGE CONTAMINATION ON SWEPT WINGS

[ETUDE DE LA TRANSITION ET DE LA CONTAMINATION DE BORD D'ATTAQUE SUR ALLES EN FLECHE]

by

D. Arnal

J.C. Juillen

AGARD-CP-438, Paper 6 (1988)

Translated by
J.D. Southon

Translation edited by
C. Betts

AUTHORS' SUMMARY

This study is concerned with an experimental investigation of the different ways in which turbulence appears in an incompressible laminar boundary layer on a swept wing. Transition is detected by the use of hot films attached to the model. The results of two series of measurements are given: in the first, the sensors are placed along the chord and the recorded signals allow the analysis of problems in streamwise and crossflow instability, and leading edge contamination. In the second series of experiments, hot films are distributed along the span, close to the leading edge. Leading edge contamination is studied in detail and possibilities of relaminarisation are considered.

LIST OF CONTENTS

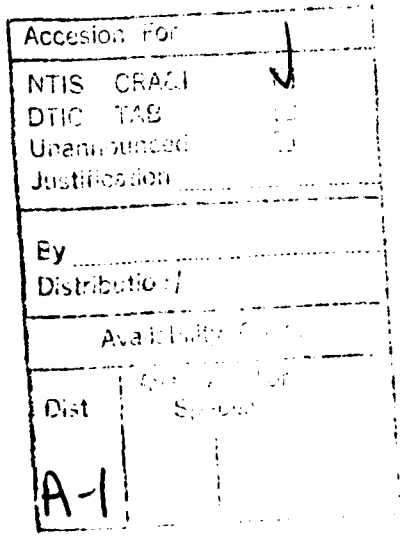

1 INTRODUCTION

A swept wing of infinite span represents the simplest case of three-dimensional flow. As shown in Fig 1, two systems of co-ordinates are generally defined: one (X, Z, y) is related to the wing, while the other (x, z, y) is related to the external flow. In both cases, the y direction is normal to the wall and the other co-ordinates are measured along the aerofoil, starting at the geometrical leading edge and perpendicular to it. The components of mean velocity are denoted (U, W, v) in the (X, Z, y) system, and (u, w, v) in the (x, z, y) system. The velocity profiles u(y) and w(y) are referred to respectively as the streamwise and crossflow profiles. Outside the boundary layer, $w_e = 0$.

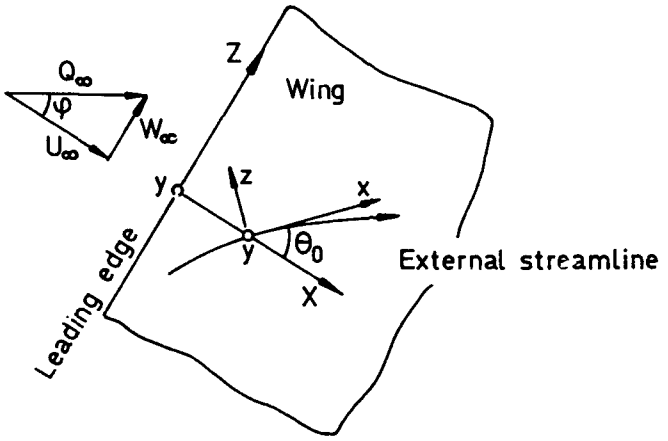

Fig 1 Geometry and notation

Using this geometry, the fundamental hypothesis is that derivatives in the direction Z of the span are zero. It follows that the component W_e of the external velocity is constant over the whole wing and equal to $W_\infty = Q_\infty \sin \varphi$ (see notation in Fig 1). If the distribution $u_e(X)$ is known, for example by measurement of static pressure, it is possible to deduce the distribution $U_e(X)$ from the equation:

$$U_e^2(X) = u_e^2(X) - (Q_\infty \sin \varphi)^2 \qquad (1)$$

In a perfect fluid, it may be shown that the profile $U_e(X)$ is that which would occur on an unswept wing situated in a flow $U_\infty = Q_\infty \cos \varphi$. In particular, $U_e = 0$ along the attachment line, the distinct flow line which separates the flows of the upper and lower surfaces.

Even if a swept wing of infinite span has simple geometry, the process of transition may turn out to be considerably more complex than for two-dimensional configurations. In fact turbulence may arise from three different mechanisms: streamwise instability, crossflow instability, and leading edge contamination (v. for example, Poll[1], Arnal[2], Saric and Reed[3]).

Streamwise instability is related to the properties of the streamwise profiles $u(y)$. Since these resemble the classical Falkner-Skan profiles, it is similar to that associated with two-dimensional flow and is the cause of transition of decelerated flow. However, the inevitable presence of a point of inflection in the crossflow profiles $w(y)$ may render these very unstable in those regions where they develop most rapidly, *ie* in the region of the leading edge. Crossflow transition is encountered mostly in accelerating flows.

From a practical point of view, the prediction of streamwise and crossflow transition may be made by applying simple criteria[4] or by the use of the linearised theory of laminar instability. The latter technique consists of calculating the growth of unstable frequencies and placing the theoretical transition at the point where the most dangerous frequency has grown by a ratio e^n, with n in the approximate range 7 to 9.

The third transition mechanism referred to above, leading edge contamination, is of a very different nature. Taking the simple example of a swept wing, if this is influenced by a solid surface (fuselage, tunnel wall), the turbulence convected on to this wall may become propagated along the attachment line and possibly render the wing completely turbulent. This basically non-linear phenomenon is an example of what Morkovin has called a "bypass"[5], in the sense that it cannot be treated by the laminar theory of instability. Under incompressible conditions, experiment has shown that the appearance of contamination is determined by the value $\overline{R}$ of the Reynolds number calculated for the attachment line

$$\overline{R} = \frac{W_e \eta}{\nu} \tag{2}$$

ν and η represent respectively the kinematic viscosity and a characteristic length defined by

$$\eta = (\nu/k)^{1/2} \quad , \quad \text{with} \quad k = (dU_e/dX)_{X=X_p} \quad , \tag{3}$$

where X_p is the ordinate of the attachment line. Generally, k is related to the local radius of curvature of the wing. It is a result of a large number of experiments that, if $\overline{R}$ is less than 245, the turbulence arising from the wall is suppressed and disappears more or less quickly along the attachment line. If this is not the case, there is contamination, an increase in the magnitude of turbulent phenomena which end up occupying the whole of the leading edge. This simple criterion, used by Pfenninger since 1965[6], has since that time been largely confirmed (Gaster[7], Cumpsty-Head[8], Poll[9], for example).

This article outlines two series of experiments in the F1 and F2 wind tunnels of the ONERA Fauga-Mauzac centre, carried out in order to check the methods of calculation of transition on swept wings. During the first series of measurements carried out on a wing

with a cambered leading edge (F2 wind tunnel) the three forms of transition were studied. During the second series of experiments, conducted on another wing in the F1 wind tunnel, an analysis was made in greater detail of the problems of leading edge contamination and of possible relaminarisation.

2 EXPERIMENTS ON A WING WITH CAMBERED LEADING EDGE (WING No.1)

2.1 Experimental arrangement and method of measurement

These experiments were carried out in the F2 wind tunnel, which has a test section of 1.4 m × 1.8 m and a length of 5 m. A detailed description is given at Ref 10. The air flow is provided by a fixed-bladed fan of variable speed, giving an air velocity in the range from zero to 100 ms^{-1} within the section. External turbulence is less than 0.1%.

The model is a wing having an ONERA D aerofoil and a C chord of 0.3 m normal to the leading edge. It has a leading edge cambered between 0 and 20% chord. The presence of this leading edge obviously contributes to pressure distributions which differ from those observed on a classic ONERA D aerofoil. The wing is attached to a half-body, which is in turn attached to one of the vertical walls of the section. Fig 2 shows the aerofoil and a diagram of the experimental arrangement in the section.

Three kinds of measurement were carried out: pressure distribution at the wall, flow visualisation by sublimation, and analysis of the signals provided by the hot films. The hot films were attached to the model at between 2.5% and 86% chord, and their signals were recorded for a large number of combinations of the three parameters, φ, α, and Q_∞, respectively sweep angle, geometrical angle of incidence and nominal flow velocity in the section. The positions of the hot films are shown in Fig 2b; they were chosen in order to avoid interactions between neighbouring sensors. The absence of interference between sensors was confirmed by comparing the transition positions indicated by the hot films and by flow visualisation at the wall, and the results were shown to be identical.

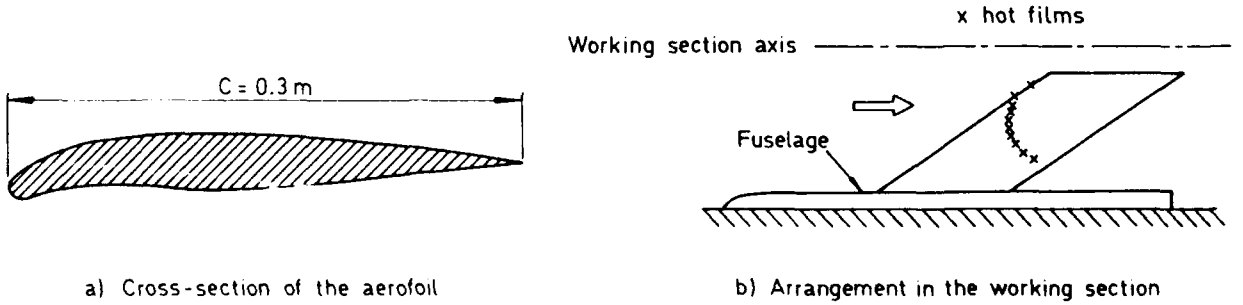

Fig 2 Experimental arrangement in the F2 tunnel

2.2 Configurations studied

Three sweep angles (φ = 49, 55 and 61°) and four geometrical angles of incidence (α = 0, –2, –4 and –8°) were studied. Typical distributions of the external velocity are given in Fig 3. On account of the cambered leading edge, the curves show complex variation in the region of negative pressure gradient.

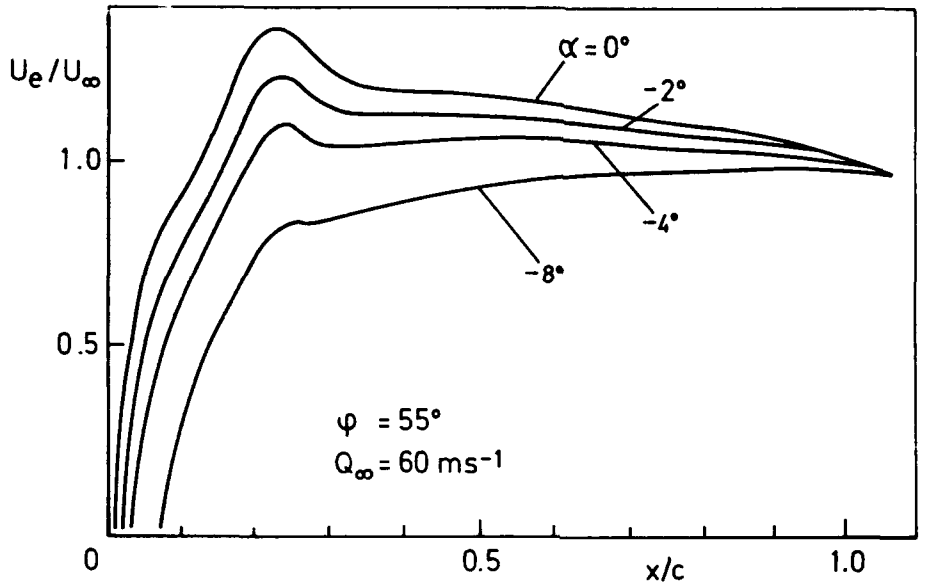

Fig 3 Examples of external velocity distribution

2.3 Results of streamwise and crossflow instability

Analysis of the results has shown that, in a large number of cases, transition occurred as a consequence of crossflow instability.

For example, Fig 4 shows the variation of the transition abscissa X_T as a function of the velocity, Q_∞, for $\varphi = 49°$, $\alpha = -2°$. The experimental data were compared with predictions derived from the separate application of criteria for transition developed at CERT/DERAT[4]. The criterion for streamwise transition is an extension of that developed by Granville; it is expressed by an equation of the form

$$R_{\theta_T} - R_{\theta_{cr}} = f(\bar{\Lambda}_2, Tu) \ . \qquad (4)$$

R_θ is the Reynolds number based on the momentum thickness of the streamwise profile; the suffixes T and cr denote the transition point and the starting point of instability. $\bar{\Lambda}_2$ is a parameter of the streamwise pressure gradient (mean Pohlhausen parameter), and Tu is the level of external turbulence.

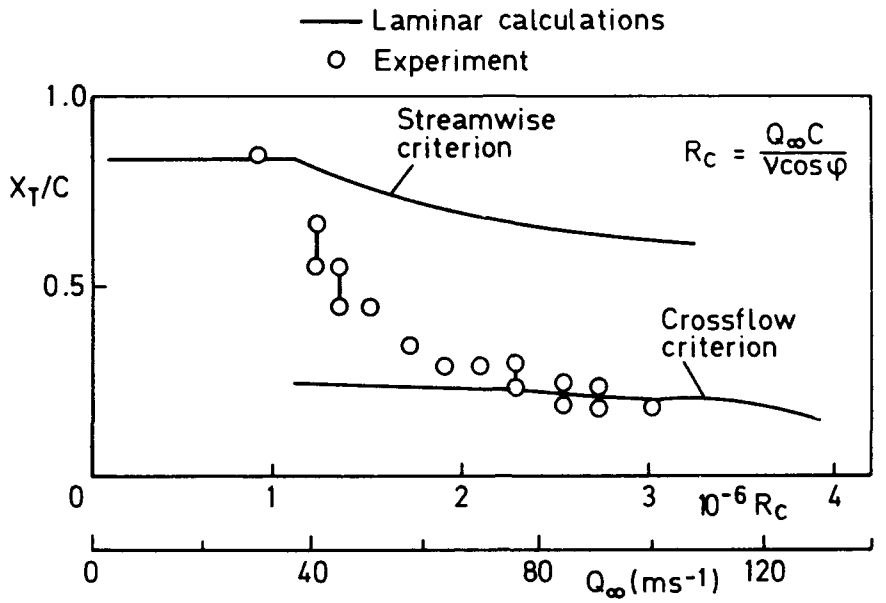

Fig 4 Variation of the transition abscissa as a function of Q_∞ (φ = 49°, α = 2°) Comparison with the results of the criteria for transition

The crossflow criterion is an empirical correlation between two complete parameters considered as the transition point: the crossflow Reynolds number

$$R_{\delta_2} = -\frac{1}{\nu}\int w dy \ ,$$

and the streamwise shape parameter H_{12}.

In the region where the flow is strongly accelerated (X/c < 0.25), the results of applying the crossflow criterion are in good agreement with the measurements. However, further downstream where the flow is decelerated, the hot films detected bursts of turbulence not predicted by the criteria. As shown in Fig 4, the transition points derived from the streamwise criterion are situated well downstream of the experimental results. Discussion of this problem may be considered from two aspects:

(a) the criteria were established from experiments in which the transition was the result of instabilities which were wholly either streamwise (x direction) or crossflow (z direction). It is possible that, between 25% and 90% chord, the most unstable directions change progressively from the z direction to the x direction. Only rigorous calculations of stability, associated with the e^n method, may then predict transitions of an intermediate type. Such an approach was adopted by Cebeci *et al*[11], and the results which they achieved are to be presented in another paper in this congress.

(b) The classical theory of linear instability, as well as the semi-empirical criteria, assume that there is no interaction between streamwise and crossflow

instabilities. Theoretical research such as that conducted by H. Reed[12] has shown that stationary waves resulting from crossflow instability may double the magnification coefficients of streamwise instabilities, and consequently lead to premature transition. These problems of interaction are of course very difficult to take into account in stability calculations. They may be introduced in an empirical manner into the streamwise criterion by modifying, for example, the pressure gradient parameter by a function of R_{δ_2} . Such work has been carried out at CERT/DERAT and has led to an improvement in prediction[13]. However, the limited number of measurements available to support this modification does not allow a definite conclusion to be reached.

2.4 Results of leading edge contamination

In this series of experiments, it was assumed that leading edge contamination appeared when turbulent fluctuations were detected on the upstream hot film, placed throughout at $X/c = 0.025$, although the abscissa X_p of the attachment line varied appreciably as a function of incidence.

Fig 5 shows some examples of fluctuating signals obtained for $\varphi = 55°$, $\alpha = -8°$ and two values of velocity Q_∞ . For each value of the latter, the signals obtained from the ten hot films were simultaneously recorded. Measurements of wall pressure indicate that the attachment line is situated at $X/c = 0.05$.

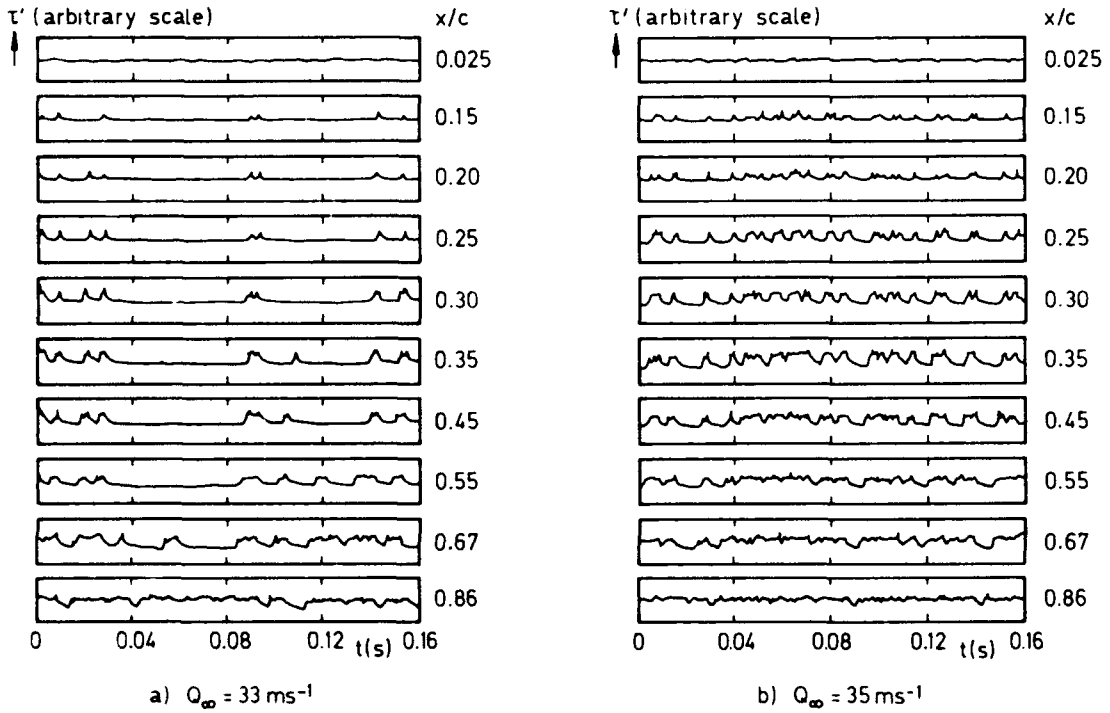

Fig 5 Examples of fluctuating hot film signals

At the lower speed ($Q = 33\ ms^{-1}$, Fig 5a) the region of the leading edge remains laminar, but a large part of the wing is "contaminated" by turbulent spots arising from the area of the junction between the wing and fuselage. An explanatory diagram of the situation is given in Fig 6: turbulent structures are created at the root by the turbulent boundary layer of the fuselage, and as R is too small, they cannot develop along the attachment line, but those that are convected along the line of external flow are detected by the hot films downstream. It is also to be noted that the recordings allow the signatures of distinctive spots to be followed in the X direction. However, as the external streamline was almost perpendicular to the row of hot films, it was not possible to calculate the convection velocity of the spots. It is noted on the recordings that, paradoxically, the beginning of a spot is often detected earlier on film n than on film n – 1 upstream. The difference between the direction of displacement of the spots and the orientation of the row of hot films allows this phenomenon to be explained; for example, in Fig 6 the spot in state 2 will be detected by hot film 9 before it is detected in state 3 by hot film 8.

When the velocity in the section was increased from 33 to 35 ms^{-1}, the number of turbulent spots grew rapidly and some turbulent bursts of air appeared at the first position. Under these conditions, the Reynolds number $\bar{R}$ was equal to 276, which is taken to be the value for the onset of contamination.

It was possible to observe leading edge contamination for five other (φ, α) pairs. The first turbulent bursts were detected on the upstream sensor at $\bar{R}_D = 258 \pm 18$ and the attachment line was completely turbulent at $\bar{R}_F = 309 \pm 12$. These values are in good agreement with those found during earlier work.

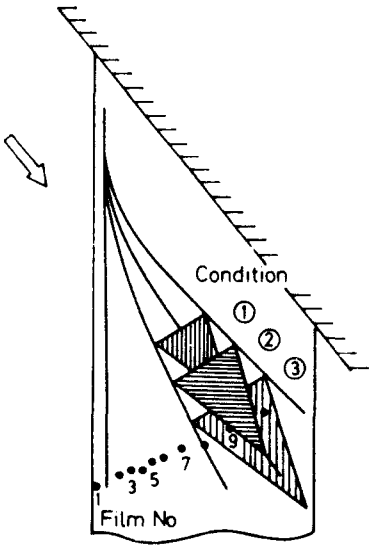

Fig 6 Interpretation of the hot film recordings

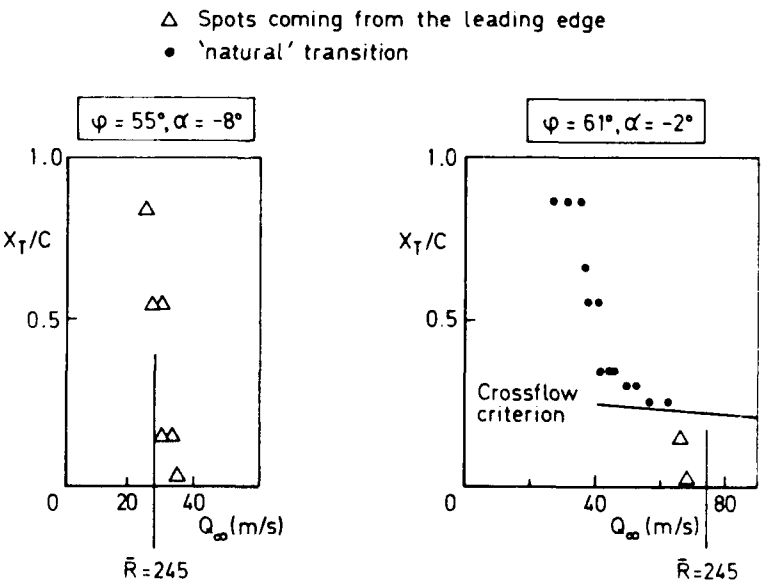

Fig 7 Transition abscissa for two cases of leading edge contamination

In actual fact, contamination may appear in a manner which differs according to the case under consideration. In Fig 7, the transition position is drawn for two experimental configurations, as a function of the velocity Q_∞. (The transition position is taken at the streamwise abscissa at which the first turbulent fluctuations are recorded). With $\varphi = 55°$ and $\alpha = -8°$ (the situation corresponding to the signals shown in Fig 5), X_T rose very rapidly from the trailing to the leading edge with neither streamwise nor crossflow instability. The situation was more complex with $\varphi = 61°$, $\alpha = -2°$. When Q_∞ increased from 40 to 65 ms^{-1}, the transition shifted slowly from 30% to 20% chord. It was initiated by crossflow instability, as shown by the application of the crossflow criterion. At higher speeds $\overline{R}$ exceeds 245 and leading edge contamination is evident. This leads to a complex situation in which two mechanisms for producing turbulence are simultaneously present. An example of this situation is shown in Fig 8, in which the velocity Q_∞ was slightly less than that at which contamination appears. Some turbulent spots were produced at X/c = 0.15 ; they occurred near to the attachment line in the region of the junction of wing and fuselage. At following positions a mixture of spots arising from the attachment line, together with those which are the result of a transition by crossflow instability, may be observed.

In the course of these experiments, development of turbulence in the X direction is of particular interest. In a second series of measurements described in the next paragraph, attention was directed towards the development of spots along the span, in areas adjacent to the leading edge.

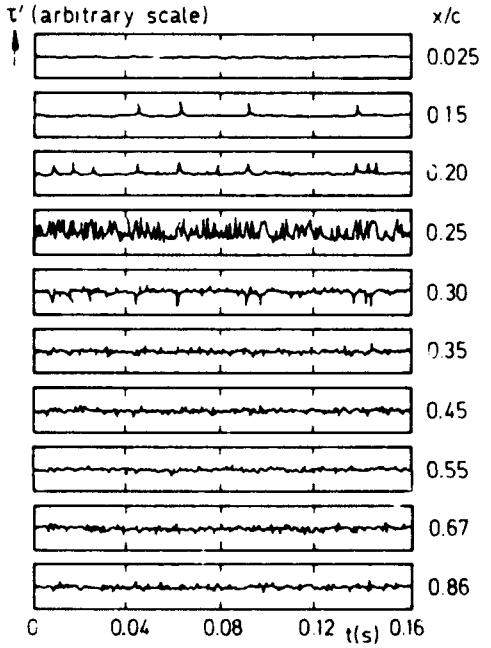

Fig 8 Transition signals for $\varphi = 61°$, $\alpha = -2°$, $Q_\infty = 66\ ms^{-1}$

Cas	φ°	α°	P_1 (bars)
A	40	2.5	3
B	40	2.5	2
C	30	2.82	3
D	30	11.3	3
E	30	11.3	2
F	30	11.3	1
G	40	10	2
H	40	10	1

Table 1 - configurations studied

Table 1 – Configurations studied

3 EXPERIMENTS ON WING No.2

3.1 Experimental arrangement

A second series of experiments was carried out in the F1 wind tunnel of the Fauga-Mausac Centre on the so-called "hyper-lift variable sweep" wing of the ONERA Aero Department. An aerofoil section and a diagram of the arrangement of the model in the wind tunnel are shown in Fig 9.

The working section is 10 m long. At its exit, the height is 3.5 m and the width, 4.5 m. The tunnel is driven by a constant-speed axial fan of variable pitch, so that the velocity in the section can be made to vary from zero to about 100 ms^{-1}. The installation operates at ambient temperature, but the total pressure may be controlled between 1 and 3 bars (v. [14]).

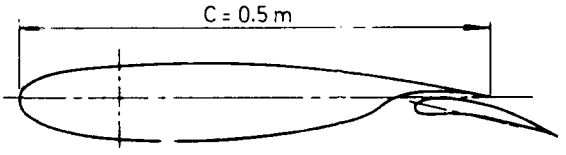

a) Section of aerofoil

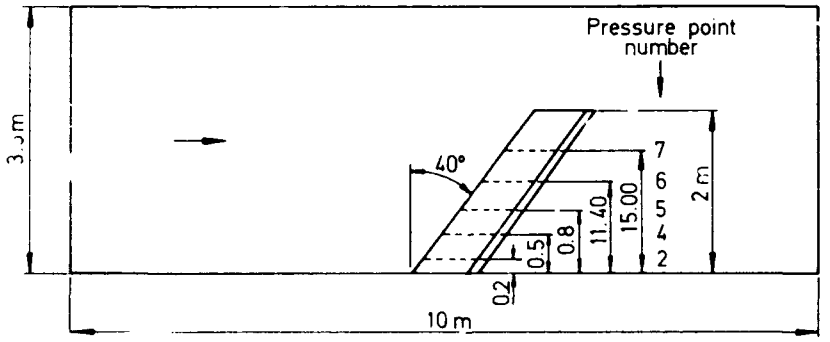

b) Arrangement in the working section

Fig 9 Experimental arrangement in the F1 wind tunnel

The model essentially comprised a wing made to the RA16 SC1 aerofoil, except between X/c = 0 and X/c = 0.20 , where an AMD-BA leading edge was employed. It was fitted with a trailing edge flap set at 10° in all the experiments (Fig 9a). The chord had a constant value of 0.5 m. With an angle of sweep $\varphi = 40°$, the upper edge of the wing was situated 2 m above the floor. The model was fitted with eight rows of static pressure sensors along the span; only the rows of sections 2, 4, 5, 6 and 7 were employed. Their location is shown in Fig 9b; at $\varphi = 40°$, these rows are parallel to the floor of the working section.

During the commissioning of the tunnel, measurements of the boundary layer were carried out at a number of points in the working section. At the fixing point of the model on the floor, measurements were obtained of classical profiles of a turbulent boundary layer, with a physical thickness of around 10 cm in the range of Reynolds numbers encountered in this study. Along the axis of the working section, the degree of external turbulence is of the order of 0.1%.

3.2 Methods of measurement – configurations studied

As in the preceding study, the hot films were the essential means of detection of transition. The transient signals simultaneously provided by eight sensors were recorded by analogue methods, then digitised and processed at the CERT computation centre.

Eight configurations, numbered A to H, were studied. Table 1 shows, in each case, the values of the angle of sweep φ , the geometrical angle of incidence α and the total pressure P_i . The configurations A, B, C correspond to a normal angle of incidence $\alpha_n = \alpha/\cos\varphi$ of 3.26° , (referred to as "low incidence"), while the five other configurations correspond to $\alpha_n = 13.05°$, (referred to as "high incidence").

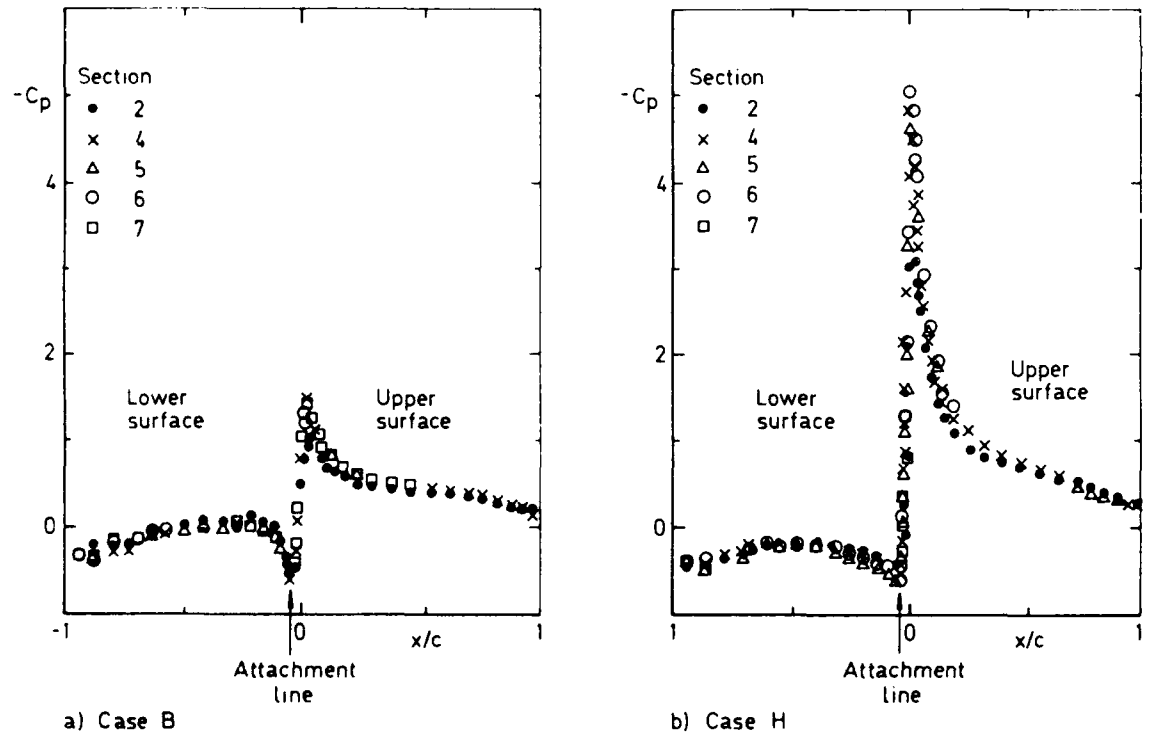

Fig 10 Examples of pressure distributions

3.3 Pressure distribution – attachment line

Fig 10 shows the distributions of the pressure coefficients C_p for two typical examples of low (case B) and high (case H) incidence. The measurements obtained at

sections 2, 4, 6 and 7 are shown as a function of X/c , where X is the curvilinear abscissa measured along the aerofoil from the geometrical leading edge. By convention, the positive values of X are associated with the upper surface and the negative, with the lower surface. The increase at the point of over-velocity on the upper surface as α increases is particularly spectacular. The point at which C_p achieves a maximum, theoretically equal to $\cos^2\varphi$ for an infinite swept wing, identifies the attachment line.

By measuring C_p , it was possible to calculate the variation of the velocity $u_e(X)$, and then, by using equation (1), the distribution $U_e(X)$, the projection of the external velocity perpendicular to the leading edge. The variations of U_e/Q_∞ as a function of X/c are shown on Fig 11 for the two cases under consideration in the previous figure. Only the measurements in the region of the leading edge are plotted, and the velocities on the lower surface are shown with a negative sign in order to enable the attachment line ($U_e = 0$) to be better visualised.

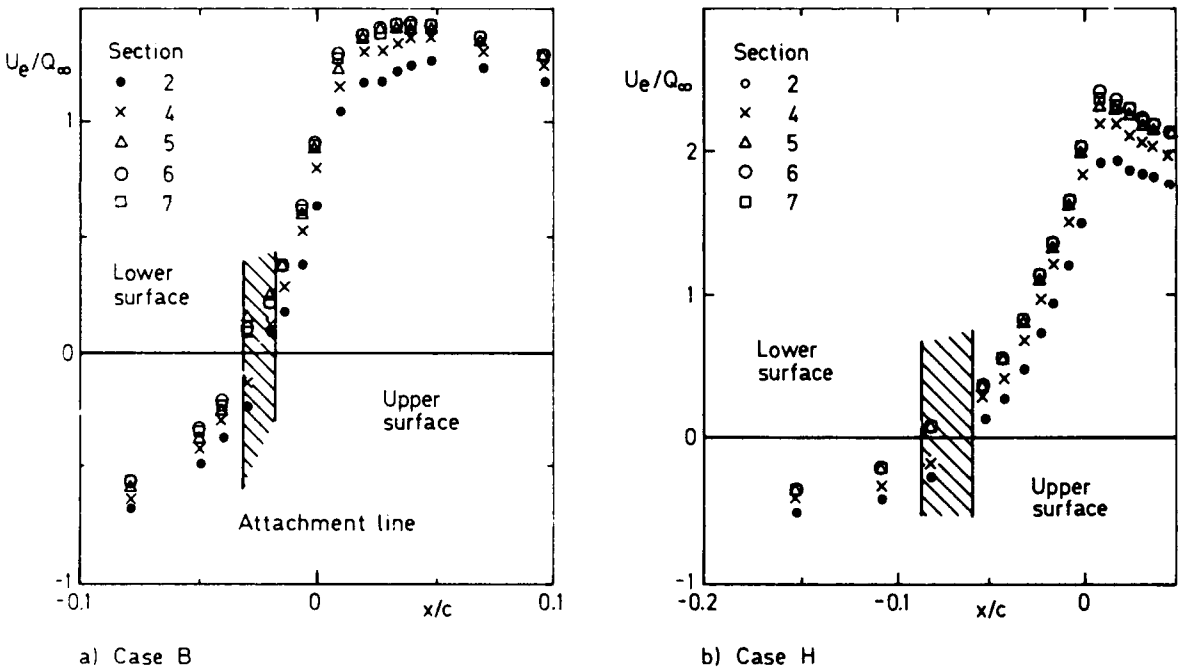

Fig 11 Distribution of velocity normal to the leading edge in the region of the attachment line

It appears that the results obtained in the different sections do not fit entirely onto a single curve and, because of this, the abscissa X_p of the attachment line varies little along the span.

3.4 First series of hot film measurements

As shown in Fig 12, for cases G and H, eight hot films were first attached along the leading edge of the wing, at approximately 2% chord on both sides of the attachment line as

determined by pressure measurements. The films numbered 2, 4, 6 and 8 were situated on the upper surface, while those numbered 1, 3, 5 and 7 were situated on the lower surface. In Fig 12 the position of the sensors along the span is shown in relation to the lines of static pressure measurements.

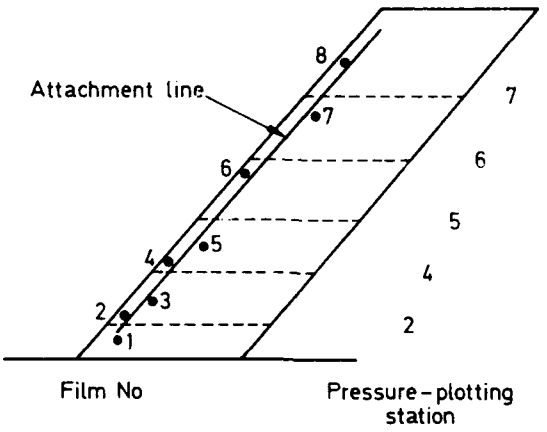

Fig 12 Positions of hot films and pressure measurement lines

During adhesion the hot films were aligned so that the sensitive element would be nearly perpendicular to the external flow streamline.

For each of the eight configurations under consideration, a progressive sweep in velocity was undertaken to define precisely the onset of contamination. For example, Fig 13 shows signals recorded in case H for $Q_\infty = 35$, 61 and 64 ms^{-1} . At the lower velocity (Fig 13a) only film 1 indicates turbulent fluctuations which arise from the turbulent boundary layer in which the hot film is situated, at the floor. At $Q_\infty = 61$ ms^{-1} , a number of "spot" type turbulent structures are recorded by film 2; they are seen to diminish in number at films 3 and 4, then to remain constant. At films 4 to 8 these spots are seen to be enlarged; from then on they develop along the attachment line, indicating the start of leading edge contamination. (Attention must be paid to the interpretation of these signals; for example, on film 8 two more spots may be counted than on film 6. In fact, the two spots at the left on film 8 also appear on film 6, but earlier in the recording). An increase of 5% in the velocity Q_∞ (from 61 to 64 ms^{-1}) leads to a very rapid growth in the number of spots, as a comparison of Figs 13b and 13c shows. At 95 ms^{-1}, all signals are fully turbulent.

Next, the calculation of $\overline{R}$ at the onset of contamination was carried out using equations (2) and (3). The critical part consisted of estimating the parameter $k = (dU_e/dX)$ at $X = X_p$. Fig 11 illustrates the difficulty of obtaining an accurate value of the velocity gradient in the region of the attachment line, with this gradient varying somewhat along the span. After smoothing of the experimental points, a mean value for k was taken on the five sections on which the pressure was measured. The onset of contamination was located at $\overline{R}_D = 251 \pm 11$, the leading edge being completely turbulent at $\overline{R}_F = 318 \pm 22$. These results are very close to those obtained in the first series of experiments.

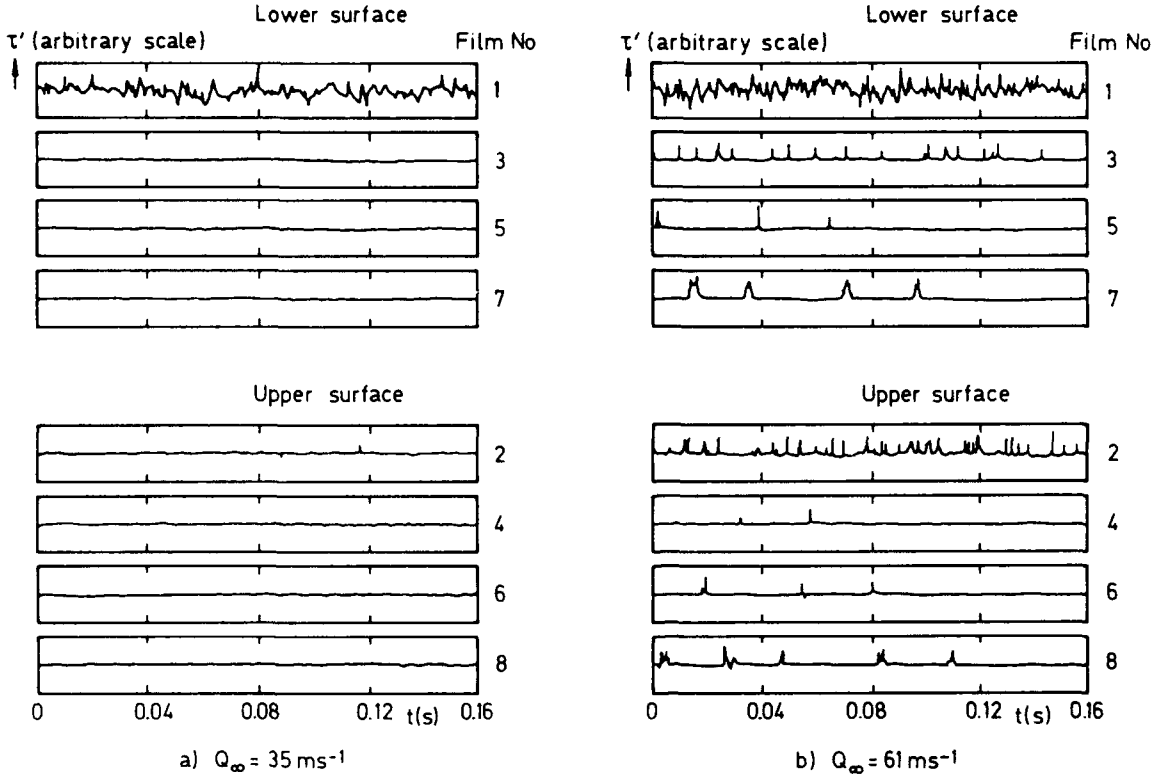

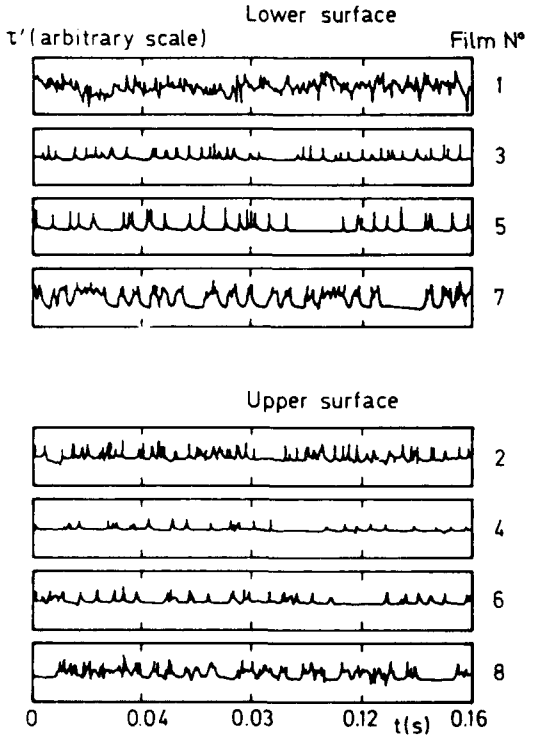

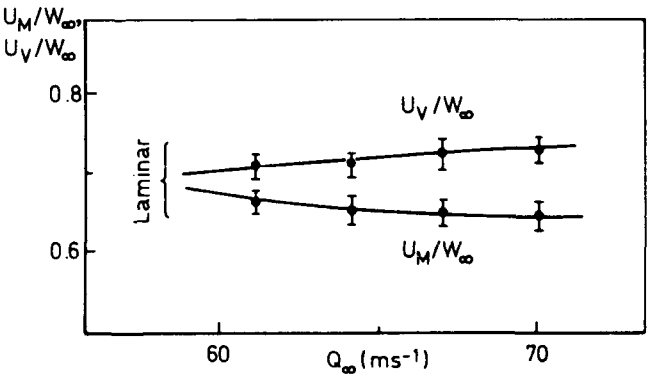

Fig 13 Signals obtained from hot films, $\varphi = 40°$, $\alpha = 10°$, $P_l = 1$ bar

Fig 14 Convection velocities of the fronts downstream (U_V) and upstream (U_M) of the turbulent spots, between films 5 and 7, case H

In the majority of recordings in which $\bar{R}_D < \bar{R} < \bar{R}_F$, it was possible to follow the movement of the indivudal spots from one hot film to another, and to derive from that the convection velocities U_M and U_V of their upstream and downstream fronts, upstream and downstream being defined with reference to the direction of increasing Z. Fig 13b illustrates this type of calculation for two spots which were followed between films 5 and 7. The results are given in Fig 14 for case H: the ratios U_M/W_∞ and U_V/W_∞ are show there as a function of Q_∞.

The lengthening of the spots indicates of course that the downstream front is moving faster than the upstream front, but the two velocities remain close at around 0.7 W_∞ : this value is in excellent agreement with the measurements of Gaster[7], who studied the propagation of artificial spots along the leading edge of a symmetrical wing. Beyond $Q_\infty = 70$ ms^{-1} , the spots become so numerous that they combine, preventing the measurement of their individual convection velocity.

When considering studies in which the flow is made up of a succession of turbulent spots and laminar zones, an important parameter is the intermittency factor γ, the fraction of the total time during which the flow is turbulent. The variation of γ as a function of Z was calculated in case H for several values of the velocity Q_∞ between 64 and 80 ms^{-1}. The results are shown in Fig 15a, where $Z = 0$ corresponds to the wing/floor junction of the working section. At hot film (Z = 12 cm), γ remains equal to unity. After that, the intermittency factor decreases as far as films 3 and 4 (Z = 40 to 70 cm), before increasing to the extremity of the wing. These results confirm the observations carried out on the fluctuating signals.

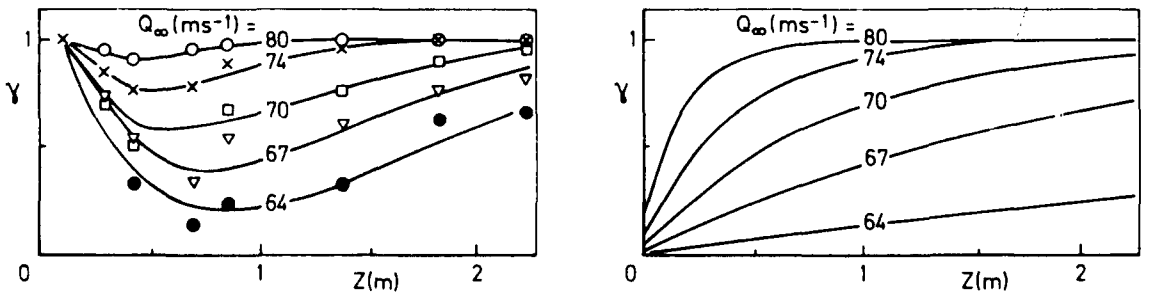

Fig 15 Intermittency factor along the attachment line, case H

Stewart and Poll[15] have recently proposed a semi-empirical equation showing the variation of γ on the attachment line as a function of the parameters $\bar{R}$ and η :

$$\gamma = 1 - \exp\left[-\left(\frac{\bar{R}-245}{106}\right)^2\left(\frac{Z}{\bar{R}\eta}+2\right)\right] \quad \text{if } \bar{R} > 245 \ . \tag{5}$$

This formula was derived from experiments in which contamination was induced by cylindrical wires surrounding the leading edge and attached perpendicularly to the attachment line, the distance Z being measured from the wire. The theoretical results given by (5) are shown in Fig 15b for the same conditions as Fig 15a. The essential differences between the two families of curves is apparent at the low values of Z, where in the current experiments, γ decreases from unity; by contrast, in the Stewart-Poll formula it increases from a non-zero but very low value. This is related to the means by which contamination is brought about, *ie* a completely turbulent boundary layer in our measurements, and a cylindrical wire in the experiments which served to establish equation (5). On the other hand, in the region in which γ increases ($Z > 0.7$ m), there is very acceptable agreement between Figs 15a and 15b, especially at $Q_\infty \geq 70\ ms^{-1}$.

3.5 Second series of hot film measurements

The next item of interest was the propagation of spots in the X direction, with the hot films remaining in the same positions in Z as before (Fig 12), but displaced along the upper and lower surfaces of the wing. The new X positions are shown schematically in Fig 16, for case H; on both surfaces of the wing, the two sets of four films were now positioned towards the maxima of the external velocity, at 10-15% chord downstream of the attachment line. The transient signals corresponding to this actual configuration are shown in Fig 17a&b, for $Q_\infty = 61$ and $70\ ms^{-1}$, respectively. On the lower surface the shape of the signals differs little from that already observed in the first series of experiments; the spots propagate from the attachment line with little modification to their structure. On the upper surface, on the other hand, individual turbulent bursts are no longer seen; at $61\ ms^{-1}$ the signals remain of a laminar nature, and at $70\ ms^{-1}$ fluctuations of low amplitude become apparent.

These observations suggest that on the upper surface the negative pressure gradient is sufficiently great to suppress the turbulent spots originating from the attachment line, at least up to a certain value of Q_∞, and relaminarisation may be referred to.

For two-dimensional flow, Launder and Jones[16] use the parameter K, to characterise possible relaminarisation in a negative pressure gradient, defined by:

$$K = \frac{\nu}{U_e^2} \frac{dU_e}{dX} \quad . \tag{6}$$

For values of K greater than 10^{-6}, experiment shows that a turbulent flow may revert to a laminar condition. It would seem, according to Beasley[17], that a value greater than about 5×10^{-6} may be necessary for the boundary layer to return effectively to this state.

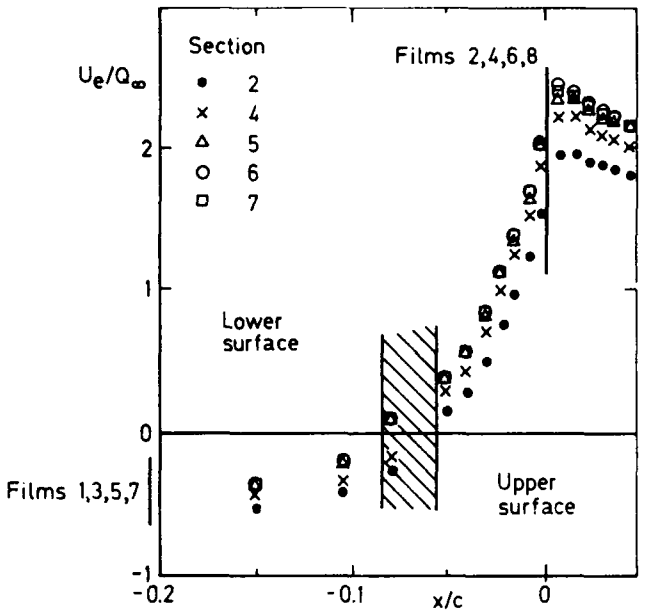

Fig 16 Position of hot films for relaminarisation study, case H

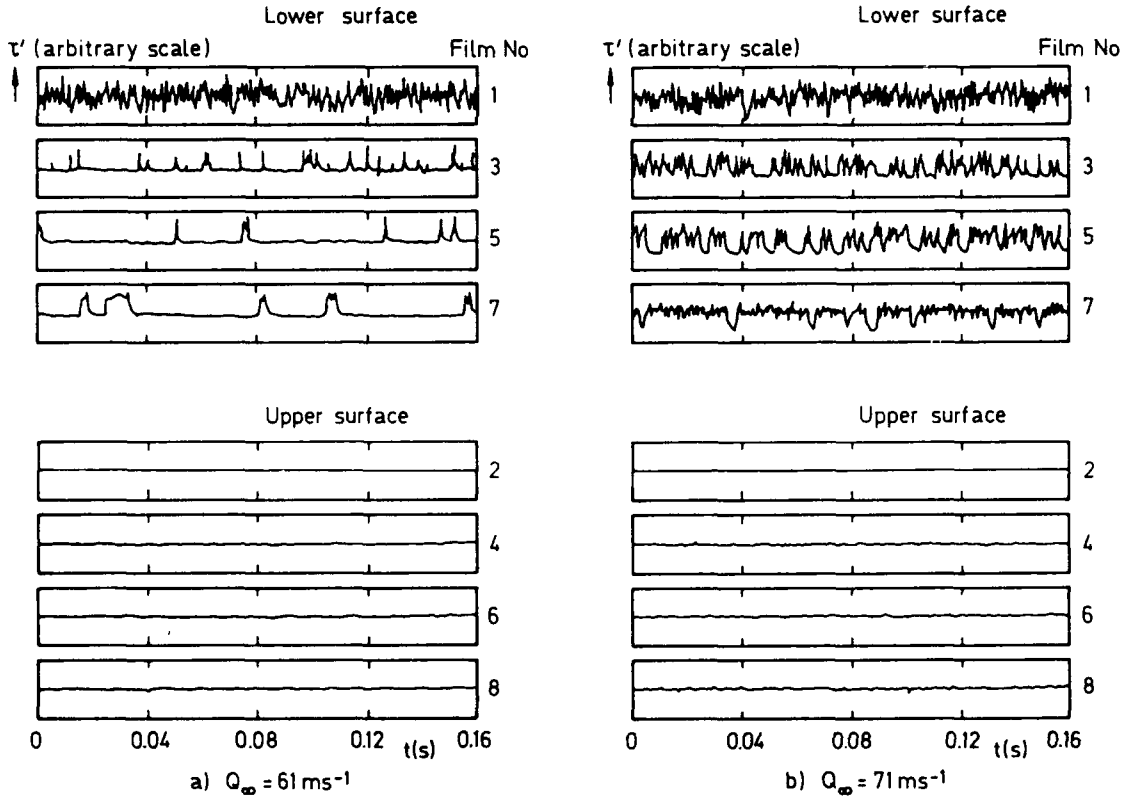

Fig 17 Signals obtained from hot films, positions as in Fig 16

In our experience, this kind of information does not exist for three-dimensional flow. One could put forward the hypothesis that the critical values given above remain valid under the conditions of calculation of the parameter K along the external streamline, *ie*:

$$K = \frac{\nu}{u_e^2}\frac{du_e}{dx} \sim \frac{1}{Q_\infty} \quad \text{for a given wing .} \tag{7}$$

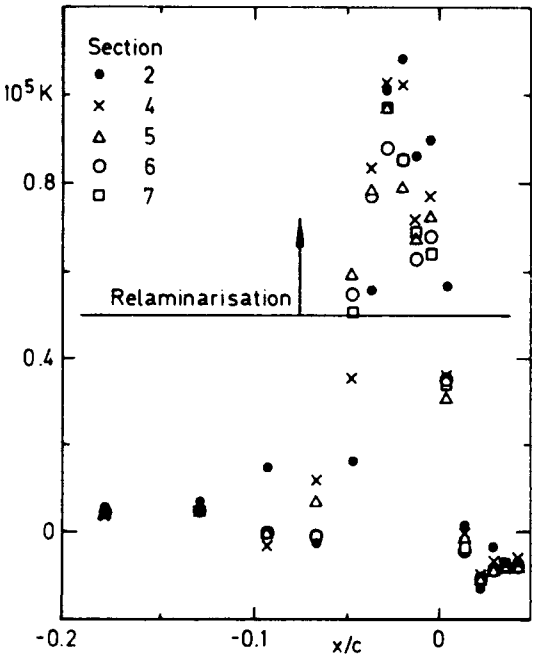

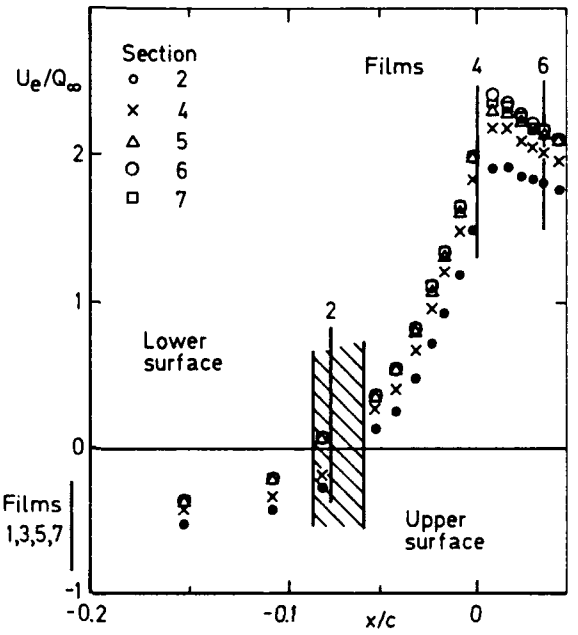

Fig 18 Variation of the parameter K , case H, Q_∞ = 60 ms^{-1}

Fig 19 Position of hot films

Fig 18 shows the experimental distribution of K under the conditions of case H, for $Q_\infty = 60$ ms^{-1} (the velocity at which contamination commences on the attachment line). On the lower surface, the value of K remains very small, while on the upper surface it reaches 10×10^{-6}, twice the minimum value required for relaminarisation. As K is inversely proportional to Q_∞, the criterion indicates that a velocity in the working section of at least 120 ms^{-1} would be required in order not to suppress further the leading edge turbulence in the accelerated region of the aerofoil. The detailed verification of the relaminarisation criterion will be the subject of later experiments.

This kind of measurement was carried out only for case H. However, calculation of the range of K showed that, at the onset of contamination its maximum value lies between 8 and 10×10^{-6} for "high incidence" configurations (cases D to H), and that it is in the region of 6×10^{-6} for "low incidence" configurations (cases A, B and C). Relaminarisation would therefore seem possible for all the combinations of α and φ considered in this study. The high values of K are attributable to the shape of the leading edge which induces particular velocity distributions; it is evident in Fig 11a&b that the concavity of $U_e(X)$ faces upwards, *ie* on the upper surface there are velocity gradients more intense than in the region

of the attachment line. With "classical" aerofoils, on the other hand, the greatest accelerations are measured on the attachment line and relaminarisation cannot occur downstream at Reynolds numbers at which contamination appears, as demonstrated by Poll's analysis for elliptic leading edges[9].

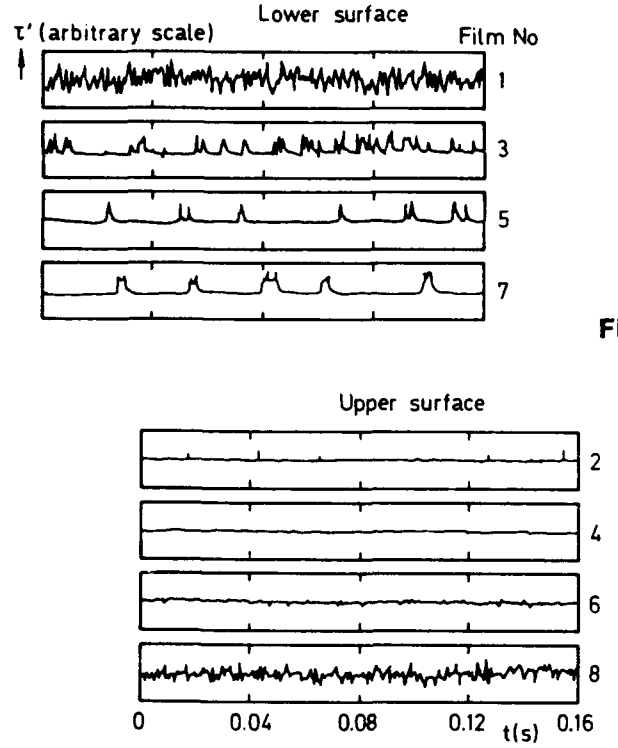

Fig 20 Signals obtained from the hot films, positions as in Fig 19, Q_∞ = 64 ms^{-1}

The hot films were finally removed and redistributed along the chord between the attachment line and 13% chord; their new arrangement is shown schematically in Fig 19, while the recordings obtained at $Q_\infty = 64$ ms^{-1} are shown in Fig 20. Two forms of transition, totally different in nature, are observed; the lower surface is swept by turbulent spots originating in the attachment line. These are suppressed on the upper surface (film 4) where the transition occurs downstream in the region of positive pressure gradient, by a streamwise instability (films 6 and 8).

4 CONCLUSION

This study has allowed a certain amount of information to be gathered on the mechanisms of transition in three-dimensional incompressible flow.

The prediction of transition induced by crossflow instability is relatively easy in regions of intense negative pressure gradient, for example, between the leading edge and the point of maximum velocity. Such a prediction may be made by the e^n method, as well as by the use of simple empirical criteria. In the case of a wing having a cambered leading edge, as considered in the first series of experiments, the problems become complicated downstream of the maximum velocity where pressure gradients remain low. The

appearance of crossflow velocity profiles in S and the simultaneous development of streamwise instability make it necessary to fall back on the theory of laminar instability.

Regarding the problem of leading edge contamination, it has been shown in the two series of measurements that the critical value $\overline{R} = 245$ may be quite confidently employed to predict the Reynolds number beyond which turbulent spots may develop along the attachment line. However, before this critical value is achieved, a significant part of the surface of the model may be swept by turbulent bursts originating from the junction of the wing and fuselage. It must also be borne in mind that contamination phenomena are not uniform along the span (γ varies in the Z direction) and, on account of this, a calculation of the boundary layer could not be carried out using the classical hypothesis $\partial/\partial Z = 0$, even if the distribution of external velocity does not vary much in the direction parallel to the leading edge.

These experiments have also shown that relaminarisation would appear to be possible if the pressure distribution downstream of the attachment line possesses streamwise gradients which are greater than along the attachment line itself.

REFERENCES

No.	Author	Title, etc
1	D.I.A. Poll	*Transition description and prediction in three-dimensional flows.* AGARD Report No.709 (1984)
2	D. Arnal	*Three-dimensional boundary layers: laminar-turbulent transition.* AGARD Report No.741 (1986)
3	W.S. Saric H.L. Reed	*Three-dimensional stability of boundary layers.* Perspective in Turbulence Studies, Springer Verlage (1987)
4	D. Arnal M. Habiballah E. Coustols	*Laminar instability theory and transition criteria in two- and three-dimensional flows.* La Recherche Aérospatiale No.1984-2 (1984)
5	M.V. Morkovin	Bypass transition to turbulence and research desiderata. Symposium "*Transition in Turbines*", Cleveland, Ohio (1984)
6	W. Pfenninger	Flow pheomena at the leading edge of swept wings. *Recent Developments in Boundary Layer Research*, Part IV, AGARDograph 97 (1965)
7	M. Gaster	On the flow along swept leading edges. *The Aeronautical Quarterly*, Vol XV III, Part 2 (1967)
8	N.A. Cumpsty M.R. Head	The calculation of three-dimensional turbulent boundary layers – Part II: attachment line flow on an infinite swept wing. *The Aeronautical Quarterly*, Vol XVIII, Part 2 (1967)
9	D.I.A. Poll	*Some aspects of the flow near a swept attachment line with particular reference to boundary layer transition.* Cranfield Institute of Technology, CoA Report No.7805 (1978)
10	D. Afchain P. Broussaud M. Frugier G. Rancarani	La Soufflerie F2 du Centre du Fauga-Mauzac. [The F2 wind tunnel of the Fauga-Mauzac Centre]. *20th AAAF Colloquium*, Toulouse (1983)

REFERENCES (concluded)

No.	Author	Title, etc
11	T. Cebeci H.H. Chen D. Arnal	A three-dimensional linear stability approach to transition on wings at incidence. AGARD meeting "*Fluid dynamics of three-dimensional turbulent shear flows and transition*", CSME, Turkey (1988)
12	H. Reed	An analysis of wave interactions in swept wing flows. 2nd IUTAM Symposium on "*laminar-turbulent transition*", Novosibirsk, USSR (1984) Springer Verlag
13	D. Arnal J.C. Juillen F. Vignau	*Transition de la couche limite. [Boundary layer transition].* Internal Technical Report (1988)
14	J. Christophe	*La soufflerie subsonique pressurisée Fl de l'ONERA. [The ONERA F1 subsonic pressurised wind tunnel].* ONERA Technical Note 158230 (1974)
15	I.R. Stewart D.I.A. Poll	An experimental investigation of the development of intermittent turbulence on a swept attachment line. *EUROMECH 28 "Boundary layer instability and transition"*, Exeter (1987)
16	B.E. Launder W.P. Jones	*On the prediction of laminarisation.* ARCCP 1036 (1968)
17	J.A. Beasley	*Calculation of the laminar boundary layer and prediction of transition on a sheared wing.* RAE Farnborough, Report No.3787 (1976)